Structural Basis for the Function of the Ribosomal L7/12 Stalk in Factor Binding and GTPase Activation

Mihaela Diaconu,[1,6] Ute Kothe,[3,6] Frank Schlünzen,[4,7]
Niels Fischer,[2] Jörg M. Harms,[4,7]
Alexander G. Tonevitsky,[5] Holger Stark,[2]
Marina V. Rodnina,[3] and Markus C. Wahl[1,*]

[1]Röntgenkristallographie
[2]3D Kryo-Elektronenmikroskopie
Max-Planck-Institut für Biophysikalische Chemie
Am Faßberg 11
D-37077 Göttingen
Germany
[3]Institute of Physical Biochemistry
University of Witten/Herdecke
Stockumer Straße 10
D-58448 Witten
Germany
[4]Max-Planck-Arbeitsgruppen für Strukturelle
   Molekularbiologie
DESY
Notkestraße 85
D-22607 Hamburg
Germany
[5]Biological Department
MV Lomonosov Moscow State University
Vorobyevy Gory
Moscow 119899
Russia

Summary

The L7/12 stalk of the large subunit of bacterial ribosomes encompasses protein L10 and multiple copies of L7/12. We present crystal structures of *Thermotoga maritima* L10 in complex with three L7/12 N-terminal-domain dimers, refine the structure of an archaeal L10E N-terminal domain on the 50S subunit, and identify these elements in cryo-electron-microscopic reconstructions of *Escherichia coli* ribosomes. The mobile C-terminal helix $\alpha 8$ of L10 carries three L7/12 dimers in *T. maritima* and two in *E. coli,* in concordance with the different length of helix $\alpha 8$ of L10 in these organisms. The stalk is organized into three elements (stalk base, L10 helix $\alpha 8$-L7/12 N-terminal-domain complex, and L7/12 C-terminal domains) linked by flexible connections. Highly mobile L7/12 C-terminal domains promote recruitment of translation factors to the ribosome and stimulate GTP hydrolysis by the ribosome bound factors through stabilization of their active GTPase conformation.

Introduction

Protein synthesis on the ribosome is promoted by a number of translation factors. Several of them, such as

initiation factor 2 (IF2), elongation factors Tu (EF-Tu) and G (EF-G), and release factor 3 (RF3), are GTPases (Bourne et al., 1991). Cryo-electron microscopy (EM) studies have revealed that the G domains of these factors interact with a region delineated by the sarcin-ricin loop (SRL) of 23S ribosomal RNA (rRNA) and a neighboring lateral protrusion, the L7/12 stalk (referred to as the stalk hereafter) (Agrawal et al., 1998; Klaholz et al., 2004; Stark et al., 2000; Stark et al., 2002; Valle et al., 2003). The stalk region encompasses ribosomal protein L11, the region of 23S rRNA that binds proteins L11 and L10 (nucleotides 1030–1124 in *E. coli*), and a complex formed by L10 and multiple copies of L7/12. (L7 is equivalent to L12 except for an acetylated N terminus. We refer to the proteins from hereon collectively as L12.)

L12 is composed of an N-terminal dimerization module and a globular C-terminal domain (CTD) connected by a flexible hinge region (Liljas and Gudkov, 1987). On *Escherichia coli* (*eco*) ribosomes, four copies of L12 are bound as two dimers via their N-terminal domains (NTD) to L10, while L10 is attached to the rRNA. Extraction/complementation experiments have demonstrated the requirement of L12 for binding of EF-Tu, EF-G, IF2, and RF3 to the ribosome and for ribosome-stimulated factor-dependent GTP hydrolysis (Wahl and Moller, 2002). Subsequent studies have shown that EF-G has increased GTPase activity in the presence of isolated L12 (Savelsbergh et al., 2000) and that specific mutations in the L12 CTD affect the binding of the EF-Tu-GTP-aminoacyl-tRNA ternary complex to the ribosome (Kothe et al., 2004). Based on these data and a comparison of the L12 CTD structure to that of EF-Ts, a model of direct, transient binding of the L12 CTD to the EF-Tu G domain has been proposed (Kothe et al., 2004; Wieden et al., 2001).

Orthologs of L10 and L12 have been identified in all biological kingdoms. L10 is usually designated L10E in archaea and P0 in eukaryotes. The eukaryotic L12 orthologs belong to two families, P1 and P2, which in some organisms form further subfamilies. Although the proteins diverged in sequence during evolution (Figure 1A), it is believed that they preserved the overall one (L10 orthologs) to four (L12 orthologs) stoichiometry and their roles in factor-related functions (Gonzalo and Reboud, 2003; Wahl and Moller, 2002).

L10 and L12 are disordered or absent from recent crystal structures of 50S ribosomal subunits (Ban et al., 2000; Harms et al., 2001) and 70S ribosomes (Yusupov et al., 2001). On the other hand, cryo-EM reconstructions disclose density features in the stalk region (e.g., Agrawal et al., 1998; Agrawal et al., 1999) that cannot be accounted for by the elements seen in the 50S subunit crystal structures and cannot be reliably interpreted without an atomic structure of the L10-L12 complex. Here we describe crystal structures of a complex between L10 and the NTD of L12 from *Thermotoga maritima* (*tma*) and refine the structure of the NTD of L10E from *Haloarcula marismortui* (*hma*) on the 50S ribosomal subunit. In conjunction with structural features
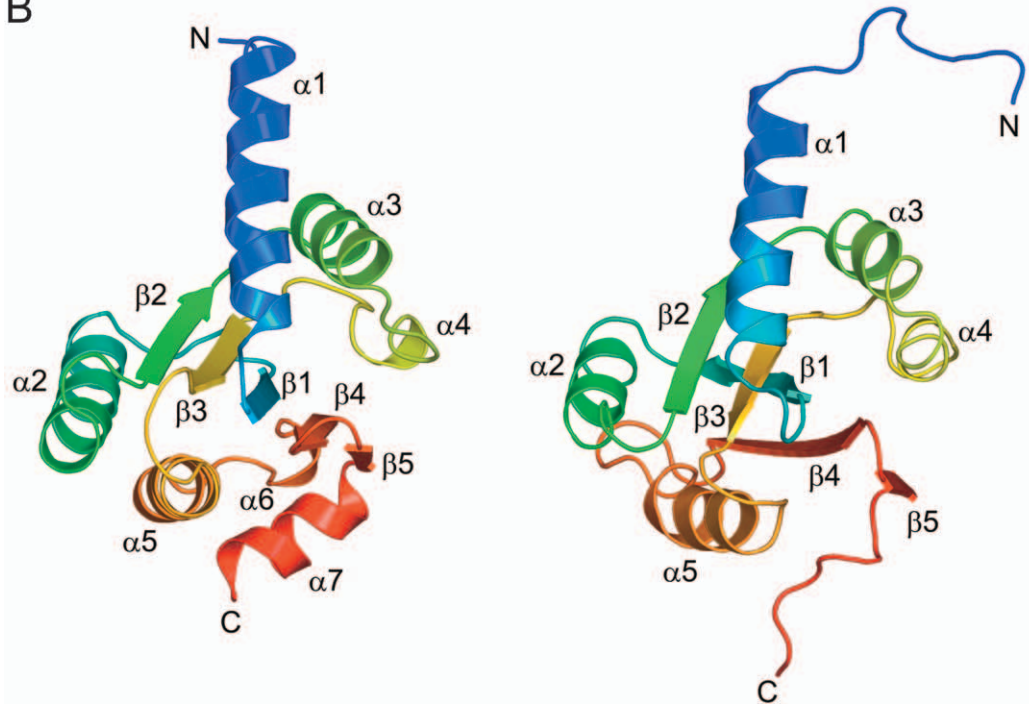
A
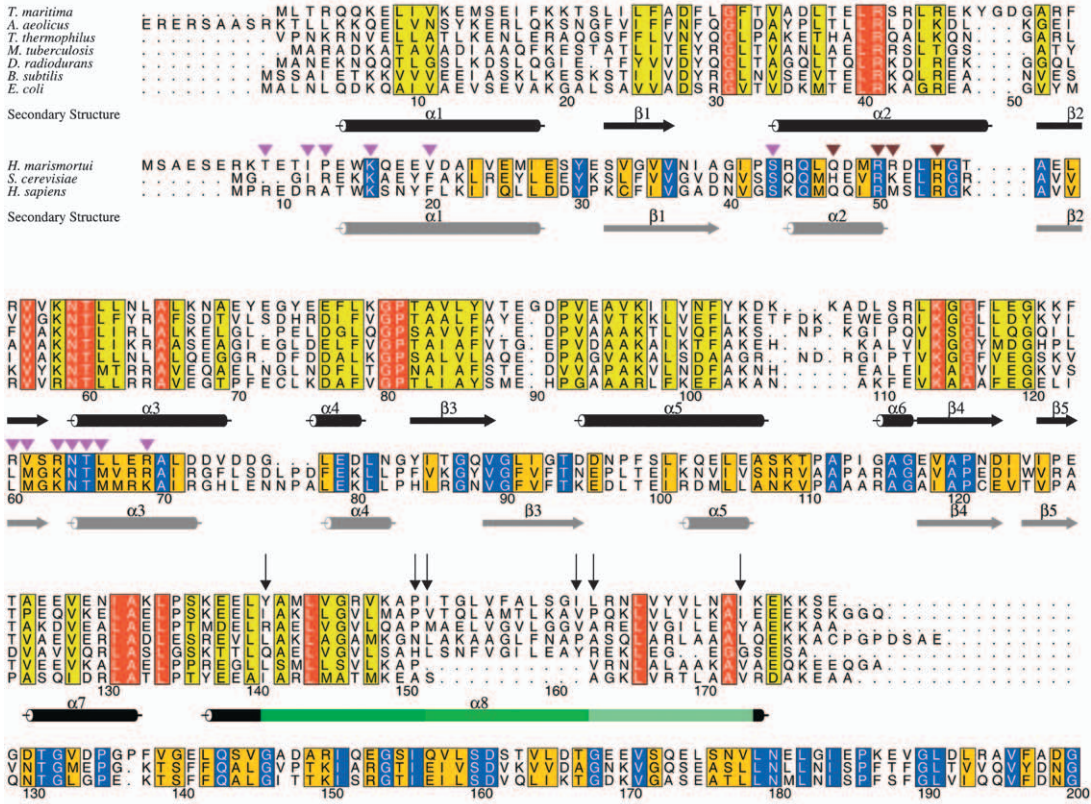
B

Figure 1. Phylogenetic Comparison

(A) Sequence alignment of bacterial L10 proteins and of *hma*L10E, yeast P0, and human P0 proteins. Secondary-structure elements of *tma*L10 and *hma*L10E, as revealed in the present crystal structures, are indicated below each block (black and gray, respectively). Sequence numberings below the blocks correspond to *tma*L10 and *hma*L10E, respectively. Within the bacterial L10 sequences, highly conserved amino acids

Results

Structure of the L10-L12$_{NTD}$ Complex

Since the flexible hinge region in L12 may hamper the production of high-quality crystals, we coexpressed full-length *tma*L10 and the NTD of *tma*L12 (residues M1–G30; L12$_{NTD}$). The proteins were copurified, and structures at 1.9, 2.1, and 2.3 Å resolution from three different crystal forms were obtained using the multiple anomalous diffraction (MAD) strategy (see Table S1 and Figure S1 in the Supplemental Data available with this article online). In all three crystal structures, one molecule of L10 was complexed with six copies of L12$_{NTD}$, the latter in the form of three dimers.

L10 comprises an α/β domain at the N terminus (Figures 1B and 2A). A long C-terminal helix (α8, K137–K174) protruding from this domain is kinked twice, at residues P151 and G161, dividing it into three ten-residue segments (Figure 1A). Each segment associates with one L12$_{NTD}$ dimer through a five-helix bundle (Figures 2A and 3A). Thus, the L10-L12 interaction region is characterized by repetition of three almost identical helix α8-L12$_{NTD}$ dimer elements.

Within each dimer, the two L12$_{NTD}$ molecules are entangled in an antiparallel fashion by extensive hydrophobic contacts. An identical arrangement of L12 molecules has previously been observed in the crystal structure of isolated *tma*L12 (Wahl et al., 2000) and subsequently in *eco*L12 in solution (Bocharov et al., 2004) (Figure 3A and Figure S2). In the *tma*L12 crystal structure (Wahl et al., 2000) the hinge region of one L12 molecule folds back as an α helix onto the two entangled NTDs. In the L10-(L12$_{NTD}$)$_6$ complex, this hinge helix is replaced by the ten-residue segments of L10 helix α8 (Figure 3A).

L10-L12 Interaction

The interfaces of the L12$_{NTD}$ dimers with L10 bury about 1500 Å^2 of combined surface area each. About 80% of the interface residues are hydrophobic (Figure 3B). Shape complementarity and electrostatic interactions at the periphery, such as salt bridges, hydrogen bonds, and bridging water molecules, register the L12$_{NTD}$ dimers on L10 helix α8 (Figure 3C). Loops of adjacent L12$_{NTD}$ dimers face each other and engage in four backbone-to-backbone hydrogen bonds via residues E11, L13, V15, and S16. Turns of L10 helix α8, which fall at the border of two adjacent L12$_{NTD}$ dimers, are pried apart by interdimer contacts, leading to the two kinks of helix α8. The interdimer interactions sup-

port a rigid arrangement of the three L12$_{NTD}$ dimers on helix α8 independent of the crystal environment.

In the three crystal structures, helix α8-(L12$_{NTD}$)$_6$ is positioned differently relative to the L10 NTD (Figure 2B), which can be described as rotations around a pivot point at the beginning of an unstructured loop connecting the L10 NTD and helix α8 (Figure 2C). The structures seem to be stabilized by the formation of different sets of salt bridges between helix α8 and the L10 NTD and between the L12$_{NTD}$ dimers and the L10 NTD (Figure 2D). These salt bridges surround hydrophobic interactions, by which a convex surface area on the first helix α8-L12$_{NTD}$ dimer element is inserted into a concave surface area of the L10 NTD (Figure 2E). These results indicate that the C-terminal helix of L10 bearing L12 is flexibly connected to the L10 NTD.

Stoichiometry of Stalk Proteins

The 6:1 (L12:L10) stoichiometry was unexpected because a 4:1 ratio has been found in *E. coli* (Subramanian, 1975). However, sequence comparisons show that helix α8 in *eco*L10 is missing one of the ten-residue L12 binding sections compared to *T. maritima* (Figure 1A), consistent with the notion that it can only accommodate two L12 dimers. In contrast, other bacteria exhibit a length and partitioning in L10 helix α8 similar to that in *T. maritima* and are expected to maintain a L10-(L12)$_6$ complex (Figure 1A). In order to confirm the L12 copy number in *T. maritima*, we produced a recombinant full-length *tma*L10-L12 complex. Multiangle laser light scattering indicated a molecular mass of 101 ± 2 kDa for this complex, in excellent agreement with the predicted mass of 102.6 kDa for a L10-(L12)$_6$ complex (Table S2). A recombinant full-length *eco*L10-L12 complex showed a mass of 68 ± 2 kDa, as compared to 66.8 kDa predicted for a L10-(L12)$_4$ composition. We also quantified the amounts of L12 on the ribosomes from *T. maritima* and *E. coli* by immunoblots. As expected, *E. coli* ribosomes contained four copies of L12. In contrast, *T. maritima* ribosomes contained six copies of the protein (Table S2; Figure S3). Thus, the length and sequence of L10 helix α8 determines the number of L12 copies per ribosome. Except for the deletion of one of the three repetitive elements in helix α8-L12$_{NTD}$, the high degree of overall sequence conservation (Figure 1A) suggests that the L10-L12 complex of *E. coli* ribosomes closely resembles the L10-L12 complex of *T. maritima*.

Conserved Mode of L10 Ortholog Binding to rRNA and L11

An important question is how the L10-L12 complex is situated on the 50S ribosomal subunit. Using a density modification procedure and published structure factors for the 50S subunit from *H. marismortui* (PDB ID code

are colored red, intermediately conserved positions yellow. In the L10E/P0 block, identical residues are shown in dark blue, conserved residues in orange. Residues of *hma*L10E that interact directly with 23S rRNA are labeled with a magenta triangle. Residues that contact protein L11 are labeled with a brown triangle. The three segments of helix α8 in *tma*L10 that associate with L12$_{NTD}$ dimers are indicated by different shades of green. Above this element, arrows indicate hydrophobic residues of L10 that stack with the F29 side chains from the L12$_{NTD}$.

(B) Ribbon plots of *tma*L10 (left) and *hma*L10E (right) NTDs in a similar orientation. The proteins are colored blue to red from N to C terminus. Secondary-structure elements are labeled. All structure figures were prepared with PyMol (http://pymol.sourceforge.net/).
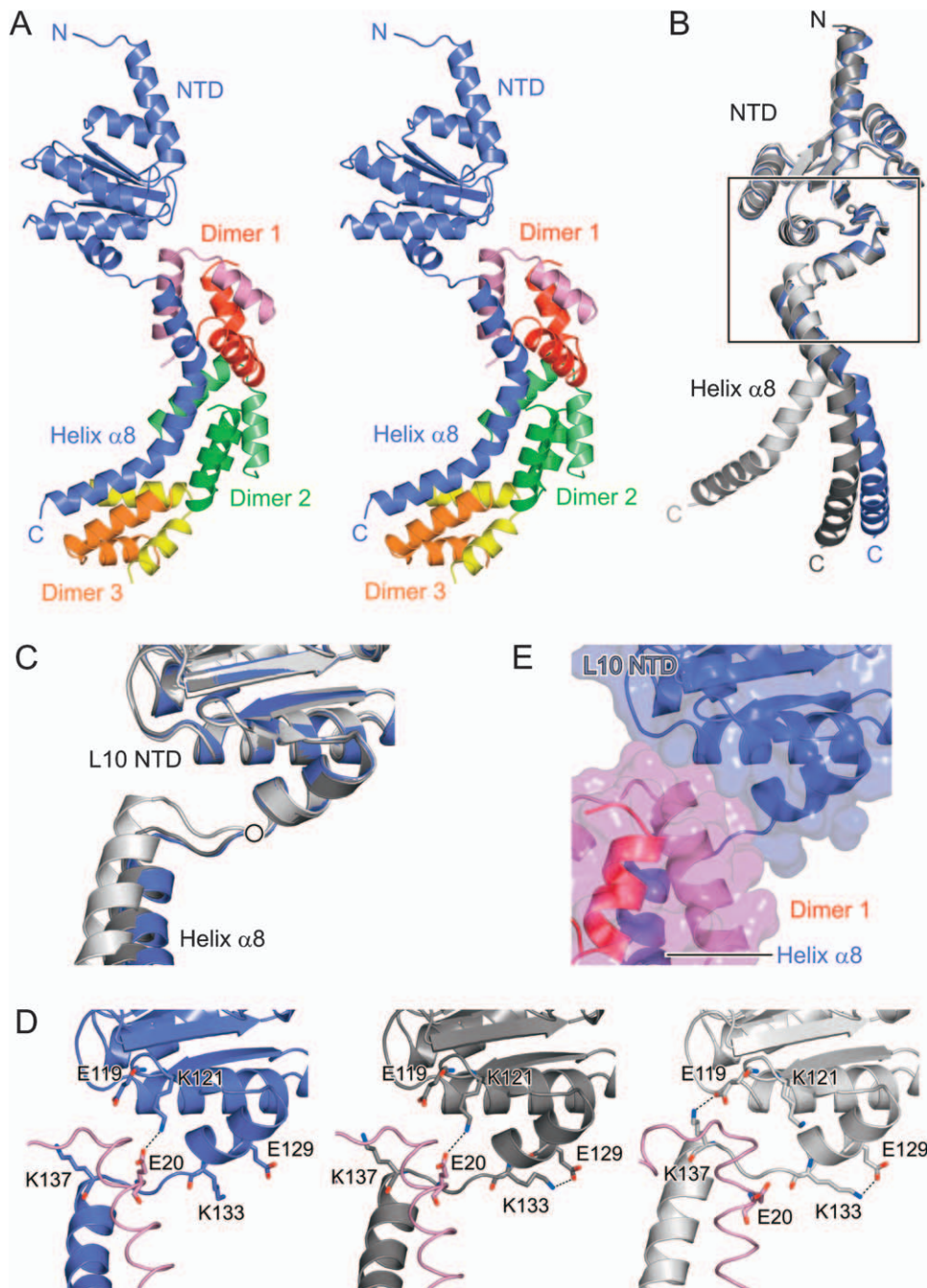
Figure 2. Structure of the Bacterial L10-(L12$_{NTD}$)$_6$ Complex

(A) Stereo view of the overall structure of the *tma*L10-(L12$_{NTD}$)$_6$ complex showing the L10 NTD at the top and three L12$_{NTD}$ dimers (protomers colored pink/red, light green/dark green, or yellow/orange, respectively) bound to the C-terminal helix α8 of L10 (purple) at the bottom.

(B) Superposition of L10 from the three crystal structures aligned on the NTDs showing the flexible attachment of helix α8 to the L10 NTD. L12$_{NTD}$ dimers have been omitted for clarity. Different L10 molecules are shown in purple (depicted also in [A]), dark gray, and light gray. The view corresponds to a 90° clockwise rotation about the vertical axis compared to (A).

(C) Close-up view of the flexible connector between the L10 NTD and helix α8 with the three L10 molecules superimposed and color coded as in (B). The figure is rotated 60° clockwise about the vertical axis compared to (B). The white button identifies a pivot point around which helix α8 rotates relative to the NTD.

(D) The same view of the three individual L10 molecules as in (C), with the proximal L12$_{NTD}$ molecule shown as a pink tube. Coloring: carbon, same as the L10 molecules; oxygen, red; nitrogen, dark blue. Dashed lines indicate salt bridges between the L10 NTD and the flexible connector or helix α8 and between the L10 NTD and the proximal L12$_{NTD}$ molecule, which stabilize the different conformations.

(E) A convex surface area of the proximal L12$_{NTD}$ dimer and the N-terminal part of L10 helix α8 (semitransparent pink surface) inserted into a concave surface area on the L10 NTD (semitransparent purple surface). The view is identical to (C) and (D). Color coding for ribbons is as in (A).
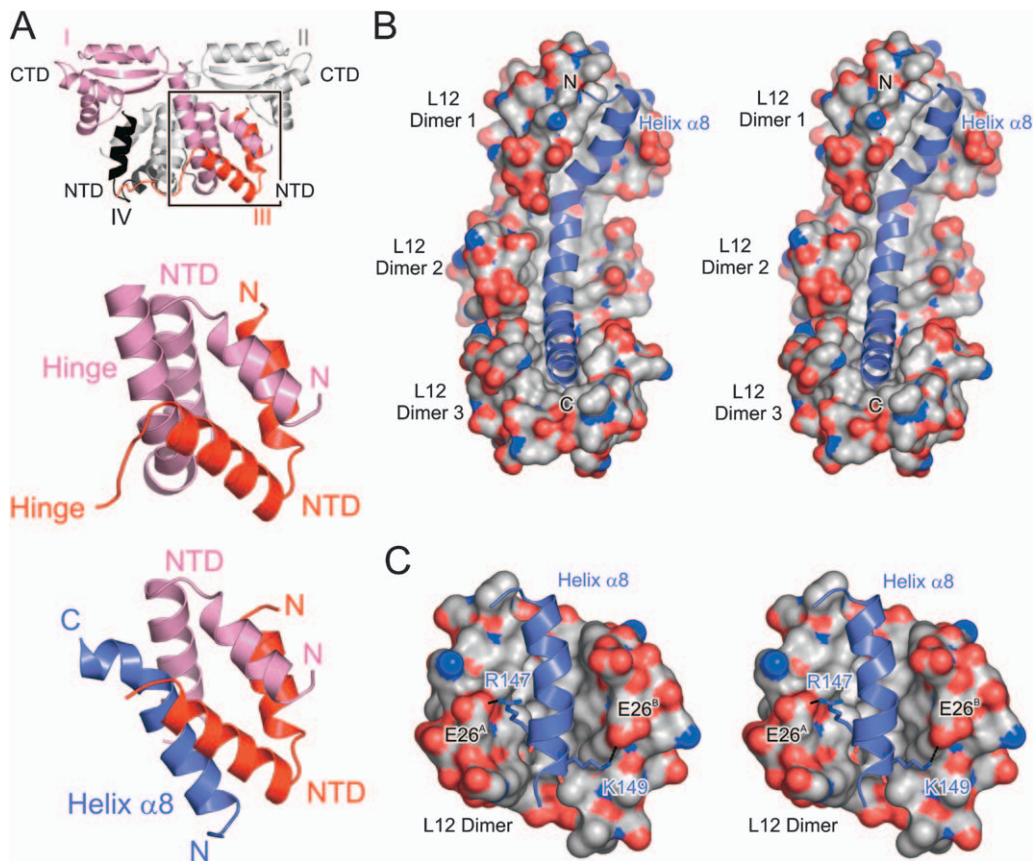
Figure 3. Details of the L10-L12 Interaction

(A) Top: heterotetrameric arrangement in the crystal structure of isolated *tma*L12 (Wahl et al., 2000) showing one type of dimerization between two full-length molecules (molecules I and II) and another between a full-length molecule and an N-terminal fragment (I and III or II and IV). Middle: close-up view of the boxed region in the top panel showing a helical hinge in complex with the NTDs in one dimerization mode. Bottom: one L12$_{NTD}$ dimer (red and pink) of the present crystal structures in complex with its L10 binding region (purple). L10 helix α8 and the α-helical L12 hinge of isolated L12 bind in a fashion similar to the identically structured L12$_{NTD}$ dimers.
(B) Stereo view of the surface of the three neighboring L12$_{NTD}$ dimers, color coded by atom type (carbon, gray; oxygen, red; nitrogen, dark blue) with the bound L10 helix α8 (purple ribbon). The image has been rotated 90° counterclockwise about the vertical axis compared to Figure 2A, revealing the hydrophobic lining of the L10 binding groove (gray interior surface) and the deep burial of helix α8.
(C) Stereo surface plot of one L12$_{NTD}$ dimer, color coded by atom type (carbon, gray; oxygen, red; nitrogen, dark blue), bound to a segment of L10 helix α8. Residues R147 and K149 of L10 engage in salt bridges with the carboxyl groups of E26 residues from the two L12 molecules (A and B) at the rim of the binding pocket.

1S72), we were able to trace the complete NTD of *hma*L10E on the 50S subunit (Supplemental Experimental Procedures; Figure S4). The *hma*L10E NTD model encompasses two helices (α1 and α3), which could be built previously (chain G in PDB entry 1S72). Despite the lack of significant overall sequence identity (Figure 1A), the fold of the *hma*L10E NTD is very similar to the NTD of *tma*L10 (Cα rmsd 2.0 Å; Figure 1B and Figure S5).

*hma*L10E employs a shallow, concave surface rimmed by helices α1 and α2 to interact with the L10/L11 binding region in domain II of 23S rRNA (Figure 4A), which comprises helices H42, H43, and H44 (nucleotides 1142–1221 in *hma*, 1038–1117 in *eco*; Figure 4B), consistent with the previous assignment of region 1028–1124 (*eco*) as the rRNA binding site of L10 (Beauclerk et al., 1984). Nucleotides U1149–G1151 (*hma* numbering; for *eco* numbering, see Figure 4B) of H42 (rRNA

region 1 in Figure 4A) are sandwiched between the N-terminal part of helix α3 (R63–T65; R69) and the N terminus/helix α1 region (T9, I12, P13, K16; Figure 4C), in excellent agreement with the protection pattern of L10 on isolated 23S rRNA (Rosendahl and Douthwaite, 1993). The β2-α3 loop (R63, N64) engages in contacts with the upper stem of H42 (nucleotides G1210 and G1211; Figure 4C; region 4 in Figure 4A). The C terminus of β2 (R60, V61) binds to the loop connecting H43 and H44 (nucleotide A1188; Figure 4D; region 3 in Figure 4A). The β1-α2 loop (S43) interacts with the short H42-H43 connector (nucleotides G1160 and A1161; Figure 4D; region 2 in Figure 4A). Thus, *hma*L10E interacts with a number of discontinuous regions of the rRNA, contacting predominantly the sugar-phosphate backbone (Figures 4C and 4D). The protein therefore seems to recognize the overall fold of the L10/L11 binding region of the 23S rRNA.

A

B

C

D

E

Hydrogen bond
Hydrophobic
1234 *H. marismortui*
(1234) *E. coli*
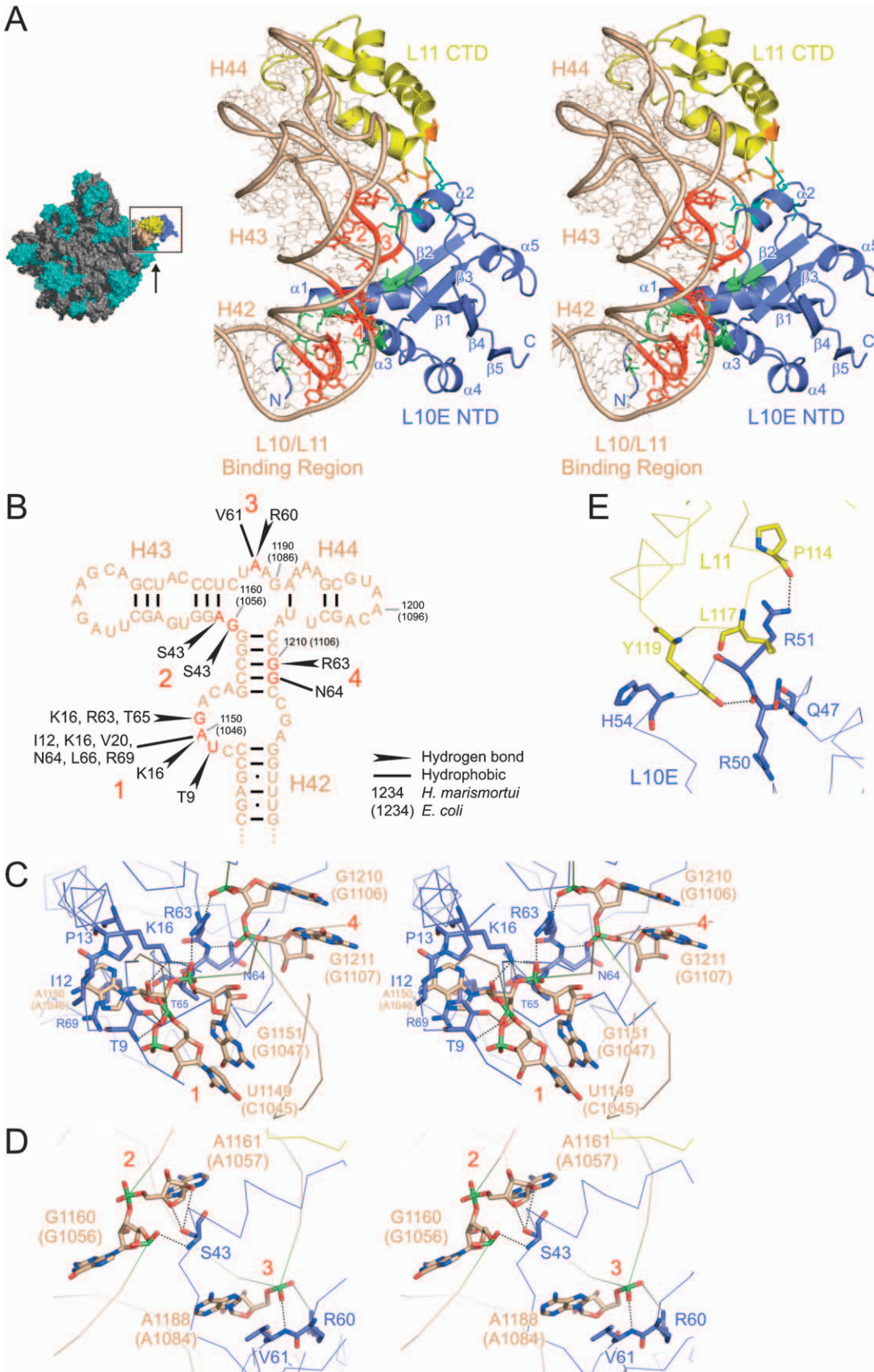
By superpositioning the *tma*L10 NTD onto the *hma*L10E NTD (Figure S5), the *tma*L10-(L12$_{NTD}$)$_6$ complex can be placed on the 50S subunit. Because the structures of the L10/L11 binding region of 23S rRNAs from *Haloarcula* and *Thermotoga* are highly conserved (Figure S5) and the protection pattern of bacterial L10 matches the contact sites seen for archaeal L10E, bacterial L10 and archaeal L10E are likely to bind in a similar fashion to rRNA, although the β2-α3 region is the only interaction site in the proteins whose sequence is conserved across the kingdoms (Figure 1A).

On the *hma*50S subunit, the L11 CTD is bound to the rRNA in the direct vicinity of the L10E NTD (Figure 4A). The loop between the two C-terminal L11 helices contacts the region between helix α2 and strand β2 of L10E. There are only a few hydrophobic interactions and two hydrogen bonds connecting the proteins (Y119^{L11}-R50^{L10E} and P114^{L11}-R51^{L10E}; Figure 4E). The L11 CTD structure is also highly conserved between bacteria and archaea (Figures S4 and S5), suggesting similar L10-L11 interactions.

Cryo-EM Reconstructions of the Stalk

To visualize the stalk in complete 70S ribosomes, we attempted to localize an L10-L12$_{NTD}$ complex in cryo-EM reconstructions of *E. coli* ribosomes. For fitting into the EM maps, we used the crystal structure of the 70S ribosome from *E. coli* (Vila-Sanjurjo et al., 2003) and a model of an *E. coli*-like L10-(L12$_{NTD}$)$_4$ complex that was generated by shortening helix α8 of *tma*L10 and omitting the peripheral L12$_{NTD}$ dimer. The 70S crystal structure was docked into the cryo-EM densities and the L10-(L12$_{NTD}$)$_4$ model was aligned with the crystal structure according to the orientation of the *hma*L10E NTD on the *hma*50S subunit.

Cryo-EM reconstructions of ribosomes at various stages of translation showed a well-defined density neighboring the L10/L11 binding region of the 23S rRNA and L11, which is consistent with the crystal structure of the *tma*L10 NTD (Figure 5 and Figures S6 and S7A–S7E). In the ribosome-EF-G-GDP complex stalled by fusidic acid (determined herein and in Agrawal et al., 1998) an elongated protuberance is seen that extends from the L10 NTD (Figure 5 and Figure S6).

The L10 helix α8-(L12$_{NTD}$)$_4$ portion can be fitted to this protuberance by a rigid-body movement of helix α8-(L12$_{NTD}$)$_4$ around the pivot point in the flexible connection to the L10 NTD (Figure 5 and Figure S6) that was seen in the crystal structures (Figure 2C). The virtual axis between the pivot point and the C terminus of helix α8 of L10 in the fitted structure is rotated by ∼25° compared to an equivalent axis in crystal structure II (Table S1). Protrusions of similar shape are visible in cryo-EM reconstructions of ribosome-RF2 complexes (Rawat et al., 2003). They can be interpreted in the same way, but with a different orientation of the helix α8-(L12$_{NTD}$)$_4$ portion (∼10° or 20° rotations around the pivot point, respectively; Figures S7D and 7E). The differences in the orientation of the helix α8-(L12$_{NTD}$)$_4$ extension in the complexes with EF-G and RF2 suggest that its position changes during translation.

In various other EM structures, little or no density beyond the L10 NTD can be discerned. The density vanishes at the flexible connection between the L10 NTD and the helix α8-(L12$_{NTD}$)$_4$ part (Figures S7A–S7C), suggesting that here the helix α8-(L12$_{NTD}$)$_4$ part adopts multiple orientations with respect to the L10 NTD.

Role of L12 CTDs in Factor Function

To address the role of L12 for the function of translation factors on the ribosome, we have used translation components from *E. coli.* This system is well characterized biochemically and is known to be representative for bacterial systems in general, in keeping with the high degree of conservation of both sequence and structure as well as the exchangeability of ribosomal components and factors (see Supplemental Data). The *E. coli* L7/12 stalk encompasses two L12 dimers that may be considered the minimal stalk structure functional in bacterial ribosomes. Early experiments suggested that L12 is involved in interactions with translation factors and GTPase stimulation (Wahl and Moller, 2002). Recent rapid kinetics and mutagenesis studies showed that the interaction with L12 promotes factor binding to the ribosome (Kothe et al., 2004; Mohr et al., 2002) and is involved in the GTPase activation of EF-Tu and EF-G (Mohr et al., 2000; Savelsbergh et al., 2000). These studies used ribosomes that were either depleted of

---

Figure 4. Binding of the L10 NTD to the 23S rRNA and to Protein L11

(A) Left: crown view of the *hma*50S subunit—L10E NTD, purple; L11 CTD, yellow; L10/L11 binding region of 23S rRNA, beige. The arrow indicates the view of the boxed area in the right panel. Right: close-up stereo view of the L10/L11 binding region of *hma*23S rRNA in complex with the *hma*L10E NTD and the *hma*L11 CTD. Sections of the L10/L11 binding region, which are contacted by *hma*L10E, are highlighted in red (denoted by red numbers 1–4). L10E residues interacting with the rRNA are in green, L10E residues interacting with L11 in cyan. L11 residues interacting with L10E are in orange.

(B) Secondary-structure diagram of the L10/L11 binding region of 23S rRNA, in which specific contacts to *hma*L10E residues are indicated. Nucleotide numbers are for *H. marismortui*, in parentheses for *E. coli*. Red numbers and residues denote the regions 1–4 (from [A]) contacted by L10E.

(C) Stereo diagram depicting the recognition of nucleotides U1149–G1151 in H42 (region 1 in [A]) by amino acids R63–T65 from the N-terminal part of helix α3 and by the N terminus of L10E (T9–K16). *E. coli* nucleotide numbers are in parentheses. R63–T65 are also in contact with the upper stem of H42 (residues G1210–G1211; region 4 in [A]). Relevant residues are shown as sticks (rRNA carbon, beige; L10E carbon, purple; nitrogen, dark blue; oxygen, red; phosphorus, green). Rotated 90° clockwise about the vertical axis relative to (A).

(D) Stereo diagram showing R60 and V61 from the C terminus of β2 of L10E interacting with the loop between H43 and H44 (nucleotide A1188; region 3 in [A]). In addition, the β1-α2 loop (S43) is depicted, which contacts the H42–H43 connecting region (nucleotides G1160–A1161; region 2 in [A]). Rotated 50° counterclockwise about the vertical axis relative to (A).

(E) Details of the L10E-L11 interaction. Amino acids involved in direct contacts between the proteins are highlighted as sticks (L10 carbon, purple; L11 carbon, yellow). Rotated 90° clockwise about the vertical axis relative to (A).
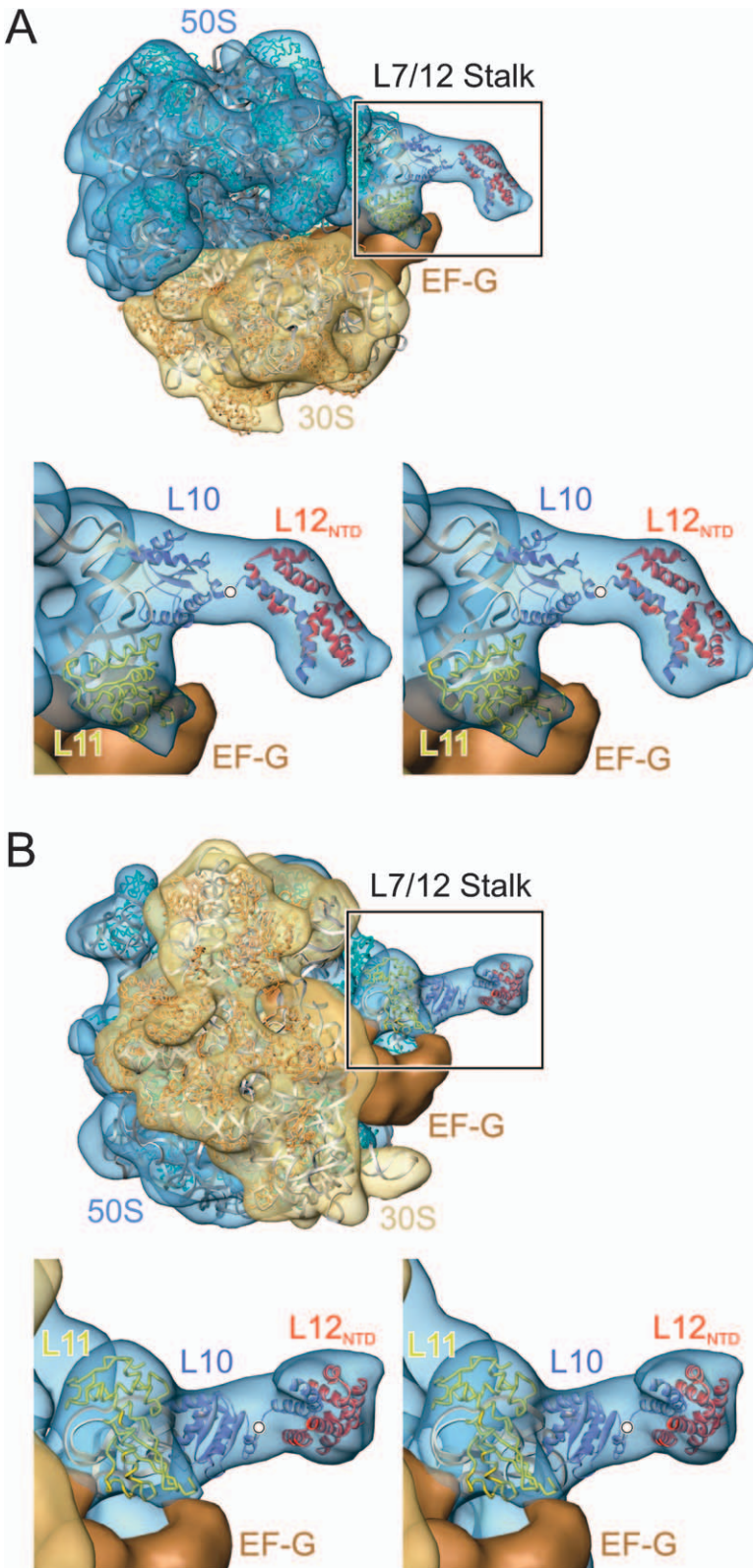
Figure 5. Localization of the L7/12 Stalk on the 70S Ribosome

(A) Fitting of the crystal structure of the 70S ribosome from *E. coli* and a L10-(L12$_{NTD}$)$_4$ complex into the cryo-EM density of an *E. coli* 70S-EF-G-GDP-fusidic-acid complex. Upper panel: overview with the 50S subunit (semitransparent blue surface) on the top and the 30S subunit (semitransparent yellow surface) on the bottom. 23S and 5S rRNAs, gray ribbons in the 50S subunit; 16S rRNA, light gray ribbon in the 30S subunit; backbone traces of 50S subunit proteins, cyan; 30S subunit proteins, orange; EF-G, brown surface. Boxed region (stalk): L10/L11 binding region of 23S rRNA, beige ribbon next to L11 and L10; L11 backbone, yellow ribbon; L10, purple ribbon; L12$_{NTD}$, red ribbons. Lower panel: close-up stereo view of the stalk region (boxed in upper panel). For clarity, only the L10/L11 binding region of 23S rRNA, L11, and the L10-(L12$_{NTD}$)$_4$ complex are shown. Relative to the arrangement seen in crystal structure II (Table S1), the helix α8-(L12$_{NTD}$)$_4$ region was adjusted by a rigid-body movement (Figure S6) around the pivot point (white button; compare to Figure 2C) to fit into the EM density.

(B) Fitting as in (A), rotated by 90°, showing a view from the 30S side. Color coding as in (A).

L12 or contained mutant L12. The contributions of the domains of L12 were so far not differentiated clearly. We therefore examined the function of the L12 CTD by first measuring the rates of factor recruitment and GTP hydrolysis with ribosomes lacking the CTD of L12. Native *eco*L12 was replaced on *E. coli* ribosomes by a

CTD deletion mutant of L12 (L12$_{NTD/hinge}$). Rate constants of the association of the EF-Tu-GTP-Phe-tRNA^{Phe} complex with ribosomes were measured by fluorescence stopped-flow (Kothe et al., 2004; Mohr et al., 2002) (Figure 6A). The rate constant of EF-Tu-GTP-Phe-tRNA^{Phe} binding to the ribosomes lacking the L12 CTD was 7 $\mu M^{-1}s^{-1}$, >10 times smaller than that observed with wild-type ribosomes, suggesting a significant contribution of the L12 CTD to factor binding. A number of single amino acid exchanges in the L12 CTD had an effect similar to removal of the whole domain (Figure 6D).

Ribosomes lacking L12 CTDs were also strongly impaired in EF-Tu-promoted GTP hydrolysis compared to wild-type ribosomes (Figure 6B). The low rate of GTP hydrolysis, about 0.4 s^{-1}, did not increase with concentration and was not limited by the binding step (expected to be 7–21 s^{-1} at 1–3 μM concentrations used in Figure 6B). The rate of GTP hydrolysis was about the same as that of ribosome cores depleted of L12 (0.2 s^{-1}; Mohr et al., 2000) and >1000-fold slower than that of intact ribosomes (>500 s^{-1}; Pape et al., 1998). The rate of GTP hydrolysis by EF-G was reduced about 600-fold by removal of the L12 CTDs (to 0.4 s^{-1}; Figure 6C) compared to intact ribosomes (250 s^{-1}; Savelsbergh et al., 2003).

To identify amino acids responsible for GTPase activation, point mutations of all conserved residues at the surface of the L12 CTD were analyzed. Several mutants showed reduced rates of ternary-complex association with the ribosome and subsequent GTP hydrolysis by EF-Tu (Figure 6D). However, the detailed analysis of the concentration dependence of GTP hydrolysis with ribosomes containing L12(R73M) (Figure 6E) suggested that the decreased rate of GTP hydrolysis is solely due to the 10-fold slower binding of the factor, as no significant effect on the rate constant of GTP hydrolysis was found. Two other mutations in the CTD, K70A and K84A, showed the same effects, i.e., slower binding and no effect on GTP hydrolysis itself (data not shown). Likewise, mutations of these conserved residues in the CTD did not affect GTP hydrolysis by EF-G (data not shown). Thus, although the CTD of L12 is required for rapid GTP hydrolysis by EF-Tu and EF-G, none of the mutated amino acid side chains of L12 is directly involved in catalysis.

Stalk Function in Factor Recruitment

Eukaryotic orthologs of L12 appear to exchange readily between the ribosome bound and free cytoplasmic pools during translation, providing a potential regulatory mechanism (Gonzalo and Reboud, 2003). We therefore asked whether such an exchange may take place on bacterial ribosomes and influence factor recruitment. To examine whether preformed L12-factor complexes could rapidly attach to the ribosome, the exchange of ribosome bound fluorescence-labeled L12 with excess unlabeled L12, or vice versa, was studied. Only very slow (less than 10% per hour) exchange between free and ribosome bound L12 was observed, independent of the absence or presence of EF-G (Figure 6F). In addition, the ratio of L12 to translation factors in the cell (Figure S3) suggests that only about 10% of the

factors would have a chance to bind to free L12 off of the ribosome. These findings disfavor models suggesting the recruitment of translation factors to the ribosome through the free L12 pool in bacteria.

Discussion

Structural Organization of the Stalk

In the present study, we have determined crystal structures of a bacterial L10-(L12$_{NTD}$)$_6$ complex and traced an archaeal L10E NTD on the 50S ribosomal subunit. We have localized the L10-(L12$_{NTD}$)$_4$ element in cryo-EM reconstructions of E. coli 70S ribosomes and elucidated the functional role of the stalk by biochemical assays. Using the crystal structures as well as published structures of a tmaL11-rRNA complex (Wimberly et al., 1999) and ecoL12 in solution (Bocharov et al., 2004), we have built a model of the 50S ribosomal subunit encompassing a complete bacterial-type stalk with either four or six L12 molecules (Figure 7). The structures of all components in the model have been experimentally determined, and the components exhibit structurally conserved overlaps with neighboring parts, which guide the model building (Figure S5).

The stalk can be divided into three structural and functional segments. The first segment is formed by the entire L10/L11 binding region of 23S rRNA, L11, and the L10 NTD and is usually referred to as the stalk base. It serves as the attachment site for the peripheral components of the stalk, positioning them in the neighborhood of the ribosomal factor binding site. The second segment is composed of L10 helix α8 in complex with the L12$_{NTD}$ dimers. The L10 helix α8-L12$_{NTD}$ part is flexibly attached to the stalk base, as seen in the three different crystal structures of tmaL10-(L12$_{NTD}$)$_6$ and in the EM analysis. It can therefore be regarded as a moveable platform that carries the L12 hinges and CTDs. The third segment consists of the L12 CTDs, which are attached to the L10 helix α8-L12$_{NTD}$ platform through the L12 hinge regions. Most likely, the L12 hinges predominantly adopt random-coil structures as in isolated L12 (Bocharov et al., 2004) because they are displaced from the L12$_{NTD}$ dimers by L10 helix α8, in agreement with recent NMR data for 70S ribosomes (Mulder et al., 2004). Thus, the flexible connection of the L10 NTD to helix α8 and the flexible L12 hinge regions connecting the NTDs and CTDs of L12 separate the three segments of the stalk and provide high mobility for the L12 CTDs. As shown by kinetic analysis, the functional interactions with the factors are performed by the CTDs of L12 that constitute the "active sites" of the stalk. Restricting the motion of L12 CTDs by hinge deletions inactivates the ribosome (Oleinikov et al., 1993), indicating that the mobility of the L12 CTDs is crucial for the activity of the stalk. E. coli ribosomes used herein for functional analyses comprise the minimal set of stalk components present in all bacteria and thus should encompass the fundamental and ubiquitous stalk activities, corroborated by the high degree of conservation of both L10 and L12 throughout the bacteria. The additional repetitive stalk element, consisting of a segment of L10 helix α8 and a L12 dimer, such as found in T. maritima, may augment the activities of L12 in certain environments
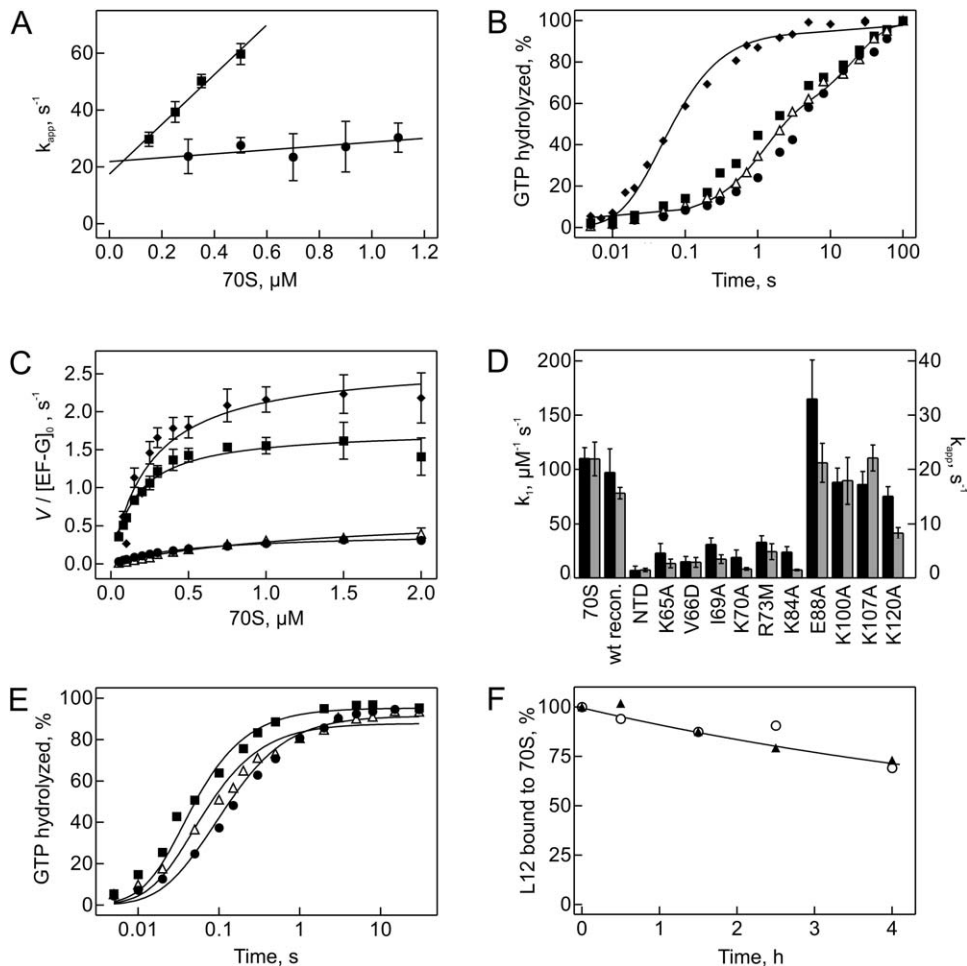
Figure 6. Functional Role of L12

(A) Contribution of L12 CTD to recruitment of EF-Tu-GTP-Phe-tRNA[Phe] to the ribosome. Apparent rate constants of ternary-complex binding to the ribosome were measured by stopped-flow with 70S ribosomes containing $L12_{NTD/hinge}$ (circles) or the full-length L12 (squares). Association and dissociation rate constants, k_1 and k_{-1}, were determined from the slope of the plot and the Y axis intercept, respectively. Rate constants of binding to $70S-L12_{NTD/hinge}$ were $k_1 = 7 \pm 3 \ \mu M^{-1}s^{-1}$, $k_{-1} = 22 \pm 3 \ s^{-1}$; those to $70S-L12_{wt}$ were $k_1 = 100 \pm 20 \ \mu M^{-1}s^{-1}$, $k_{-1} = 20 \pm 5 \ s^{-1}$. Data are represented as mean ± SD of three to seven independent experiments.

(B) GTP hydrolysis in the ternary complex stimulated by $70S-L12_{NTD/hinge}$. Purified EF-Tu-[γ-^{32}P]GTP-Phe-tRNA[Phe] and poly(U)-programmed 70S ribosomes with AcPhe-tRNA[Phe] in the P site were mixed in the quench-flow apparatus at 1 μM (closed circles), 2 μM (open triangles), and 3 μM (closed squares) each of ternary complex and 70S containing $L12_{NTD/hinge}$ or 1 μM ternary complex and native 70S (closed diamonds). The data were normalized to the same final level; the actual extent of GTP hydrolysis varied between 70% and 90%.

(C) Multiple-turnover GTP hydrolysis by EF-G. Michaelis-Menten titrations were performed by mixing 0.04 μM EF-G, 20 μM [γ-^{32}P]GTP, and increasing amounts of ribosomes. The velocity V/[EF-G]$_0$ was determined from the initial rates of GTP hydrolysis with 70S cores lacking L12 (open triangles), $70S-L12_{NTD/hinge}$ (closed circles), reconstituted $70S-L12_{wt}$ (closed squares), and native 70S (closed diamonds). Values of k_{cat} were 2.7 s^{-1}, 1.8 s^{-1}, 0.4 s^{-1}, and 0.5 s^{-1} (±0.1) for native ribosomes, $70S-L12_{wt}$, $70S-L12_{NTD/hinge}$, and 70S cores lacking L12, respectively; values of K_M were 0.2 ± 0.1 μM for native ribosomes or reconstituted $70S-L12_{wt}$, 0.6 μM for ribosomes reconstituted with $L12_{NTD/hinge}$, and 1.4 μM with 70S cores. Data are represented as mean ± SD of two independent experiments.

(D) Effect of point mutations in L12 on the rates of binding to the ribosome and GTP hydrolysis by EF-Tu. Association rate constants, k_1 (black bars, left Y axis), were determined by stopped-flow. Apparent rate constants of GTP hydrolysis, k_{app} (gray bars, right Y axis), were measured by quench-flow at 0.2 μM ternary complex and 0.7 μM ribosomes reconstituted with L12 mutants. Data are represented as mean ± SD of five independent experiments.

(E) Estimation of k_{GTPase} of GTP hydrolysis on ribosomes reconstituted with L12(R73M). Time courses were measured under conditions identical to those in (A) at 1 μM (closed circles), 2 μM (open triangles), and 3 μM (closed squares) each of ternary complex and ribosomes. Time courses were analyzed by numerical integration; smooth lines indicate fits to the following model:

$$A + B \underset{k_{-1}}{\overset{k_1}{\rightleftharpoons}} C \xrightarrow{k_2} D \xrightarrow{k_{GTPase}} E,$$
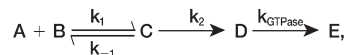
where k_1, k_{-1}, and k_2 are rate constants of ternary-complex binding to and dissociating from the ribosome and codon recognition, respectively. Parameters of the fit: $k_1 = 11 \ \mu M^{-1}s^{-1}$, $k_{-1} = 15 \ s^{-1}$, $k_2 = 100 \ s^{-1}$, $k_{GTPase} = 500 \ s^{-1}$. k_{-2} is known to be very small (0.2 s^{-1}; Pape et al., 1998) and was omitted in the calculations. With native 70S or $70S-L12_{wt}$, the rate constants are $k_1 = 100 \ \mu M^{-1}s^{-1}$, $k_{-1} = 20 \ s^{-1}$, $k_2 = 100 \ s^{-1}$, $k_{GTPase} = 500 \ s^{-1}$ (Kothe et al., 2004; Pape et al., 1998).

(F) Dissociation of L12 from the ribosome. Ribosomes reconstituted with Oregon Green 488-labeled L12 (see Experimental Procedures) were incubated in the presence of an excess of unlabeled L12 in the absence (triangles) or presence (circles) of EF-G. Analogous results were obtained when unlabeled L12 was chased from native ribosomes with an excess of labeled L12 (data not shown).
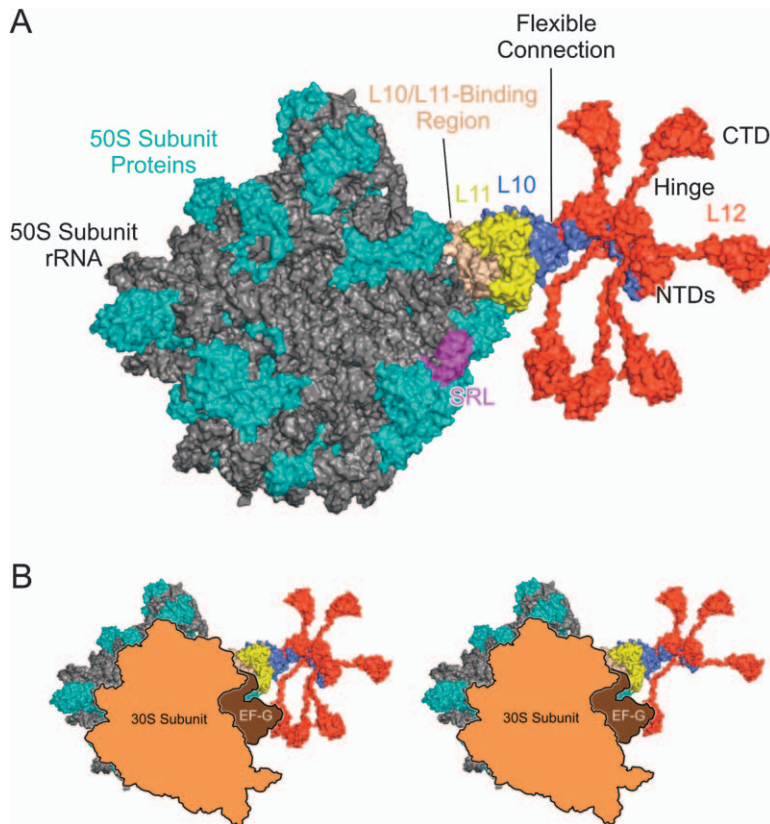
Figure 7. Models for the Organization of Bacterial Stalks

(A) Surface view of a *tma*L10-(L12)$_6$ complex modeled onto the *hma*50S ribosomal subunit (50S subunit proteins, cyan; 23S and 5S rRNA, gray; L10/L11 binding region of 23S rRNA, beige; L11, yellow; L10, purple; L12, red; sarcin-ricin loop [SRL], magenta). The L12 hinge helices are depicted in a random-coil structure. Orientation of L12 CTDs and hinge regions is arbitrary. The view is identical to that in Figure 4A, left panel, and is slightly rotated compared to Figure 5B to achieve a good view of the stalk.
(B) The same model as in (A) (left panel) or with a shortened, *E. coli*-type L10-(L12)$_4$ complex (right panel), onto which outlines of the 30S subunit (orange) and of a bound factor (EF-G, brown) are overlaid.

or even carry out yet additional functions in translation. To address these questions, purified components of the translation apparatus from *Thermotoga* are required; the tools to study the functional role of an additional stalk segment are presently being developed.

Dynamics of the Stalk during Translation
Cryo-EM analysis has shown that the extended structural elements of the stalk neighboring the base undergo rearrangements during translation (Agrawal et al., 1999). Previously, these mobile stalk elements were attributed to the hinge regions and CTDs of one L12 dimer (e.g., Dey et al., 1998). The present results suggest that the extended stalk elements revealed by cryo-EM rather represent the L10 helix α8-L12$_{NTD}$ portion of the stalk. Our data suggest that L10 helix α8-L12$_{NTD}$ and the L12 CTDs can move relative to one another and relative to the stalk base (L10/L11 binding region of 23S rRNA, L11, L10 NTD; Figure 7). Cryo-EM reconstructions identify different preferred locations of the L10 helix α8-L12$_{NTD}$ part with respect to the stalk base in ribosome-EF-G-GDP-fusidic acid and ribosome-RF2 complexes. The L12 hinges and CTDs apparently are too mobile to be located.

We can envisage two possibilities by which stabilization of the L10 helix α8-L12$_{NTD}$ part in certain functional states can be achieved. First, upon binding of factors and GTP hydrolysis, the L11 NTD may move out independently of the remainder of the stalk base due to direct contacts to the factor, as suggested for EF-G by cryo-EM (Agrawal et al., 2001). L11, the CTD of which

maintains interactions to the L10 NTD (Figure 4E), may thus constitute a bridge between EF-G and L10 NTD. It is conceivable that structural changes in L11 are communicated to the L10 NTD and could favor a particular interaction between the L10 NTD and the proximal L10 helix α8-L12$_{NTD}$ dimer element, moving around the pivot point indicated in Figure 2C. Second, direct L12 CTD-ribosome or CTD-factor contacts could form in certain functional states, thereby restricting the mobility of L10 helix α8-L12$_{NTD}$. The possibility of direct L12 CTD-ribosome interactions has previously been suggested by crosslinking (Dey et al., 1998), EM (Montesano-Roditis et al., 2001), and NMR studies (Mulder et al., 2004).

Mechanism of Factor Binding to the Ribosome
The association of both EF-Tu-GTP-aminoacyl-tRNA and EF-G with the ribosome takes place more rapidly than expected for a random encounter of two particles of this size (Rodnina et al., 1996; Savelsbergh et al., 2003). Our data identify the L12 CTDs as interaction sites for the factors. Thus, the unexpectedly high rate of factors binding to the ribosome may be explained by an increase of the encounter frequency of the ternary complex or EF-G due to multiple copies of L12, leading to a higher association rate by introducing a favorable statistical factor (Rodnina et al., 1996). This suggestion is supported by the structural model of the stalk (Figure 7): the L12 CTDs can reach far out into solution to "catch" translation factors and "hand them over" to the ribosomal factor binding site, thus efficiently restricting

factor diffusion and leading to rapid recruitment. The long, unstructured L12 hinge regions and the flexible connection of the L10 helix α8-L12$_{NTD}$ portion to the stalk base could allow the interaction of the translation factors with their ribosome binding site while being bound to the L12 CTDs. The presence of six copies of L12 on *Thermotoga* and some other ribosomes, compared to four on *E. coli*-like ribosomes, may reflect the optimization of factor binding to the particular needs of these organisms.

Mechanism of GTPase Stimulation

The L12 CTDs are responsible for an about 1000-fold stimulation of GTP hydrolysis by EF-Tu and EF-G. GTPase activation can be achieved by either promoting conformational rearrangements within the G domains of the factors that correctly position their own catalytic groups in the active site or donating additional catalytic groups in *trans*. The unique, highly conserved arginine residue in the CTD of L12 is not essential for the activation, excluding an "arginine finger"-type mechanism (present data and Savelsbergh et al., 2000). Similarly, none of the other conserved, surface-exposed amino acid residues in the CTD alone is responsible for the activation. These findings suggest that L12 facilitates GTP hydrolysis by stabilizing the GTPase transition state of the factors rather than by providing residues involved in catalysis. This mechanism of activation resembles that of the regulators of G protein signaling (RGS) that stimulate GTP hydrolysis in G$_\alpha$ proteins (for review, see Vetter and Wittinghofer, 1999). Given the high degree of sequence homology of L12 CTDs, EF-Tu, and EF-G from different bacterial species, it is likely that the RGS-type mechanism is evolutionarily conserved, at least among bacteria.

Cryo-EM reconstructions showed extensive interactions of the G domains of both EF-Tu and EF-G with the SRL of 23S rRNA (Agrawal et al., 1998; Stark et al., 2002; Valle et al., 2003), indicating that the SRL may stabilize the transition-state conformation of the factors. Single-molecule fluorescence measurements indicated that cleavage of the SRL blocks EF-Tu in a state before GTP hydrolysis (Blanchard et al., 2004). Other contacts that may contribute to GTP hydrolysis include ribosomal protein L11 and the L11 binding region of 23S rRNA (Agrawal et al., 2001). L12 represents a third ribosomal element important for stimulation of GTP hydrolysis. Through its CTD it may both facilitate positioning of the factors relative to other ribosomal components, thereby contributing to catalysis, and stabilize the active conformation of the factors. We therefore envisage that the L12 CTDs use their high freedom of motion to reach back toward the ribosome bound factors to stimulate their GTPase activity. The requirement for additional signals for full stimulation of the GTPase activity, such as the interaction with the SRL or L11, may help to avoid premature GTP hydrolysis during initial factor binding.

Experimental Procedures

Protein Production

*tma*L10 and *tma*L12$_{NTD}$ were coexpressed from two vectors in *E. coli* and purified by affinity chromatography on Ni^{2+}-nitrilotriace-

tate (NTA) (Qiagen) through a His$_6$ tag attached to the L10 N terminus. After cleavage of the tag, the complex was further purified by heat treatment (20 min, 80°C) and additional chromatographic steps. Details of these and other protocols are given in the Supplemental Data.

Full-length *eco*L12, *eco*L12 point mutants, and *eco*L12$_{NTD/hinge}$ were expressed from plasmid pGEX-5x-3-L12 in *E. coli* BL21 DE3 as glutathione S-transferase fusion proteins and purified by affinity chromatography on glutathione-Sepharose 4B as described (Kothe et al., 2004; Mohr et al., 2002; Savelsbergh et al., 2000). The cleavage of the fusion protein by factor Xa (Novagen) was carried out directly on the affinity matrix.

Crystallographic Analyses

Native and selenomethionine-derivatized *tma*L10-L12$_{NTD}$ complexes yielded two orthorhombic crystal forms and one monoclinic crystal form (Table S1). Diffraction data were collected at beamline BW6 of DESY (Hamburg, Germany). The structure of one orthorhombic crystal form could be solved by a four-wavelength MAD experiment. The structures of the other crystal forms were subsequently solved by molecular replacement. Partial models were built automatically and completed manually. Refinement of all structures was carried out by established strategies (Table S1). The structure of the *hma*L10E NTD could be built into the electron density map of the *hma*50S subunit (PDB ID code 1S72) after application of a density-modification procedure, which resembled established density-modification protocols but employed a median filter known from 2D image processing to define the molecular boundaries (for details, see Supplemental Data).

Cryo-EM Reconstructions and Fitting of X-Ray Structures

The 3D structure of an *E. coli* 70S-EF-G-GDP-fusidic-acid complex (Stark et al., 2000) was refined at 18 Å resolution using recently developed software for improved alignment and CTF correction (see Supplemental Experimental Procedures).

E. coli 30S and 50S atomic models (PDB ID codes 1PNX and 1PNY, respectively) were docked into the EM density. Excellent overall fits were obtained by adjustment of the L1 stalk ($\sim$20° rotation toward the 30S subunit) and the L11 NTD ($\sim$30° rotation away from the rRNA). The crystal structure of the *hma*50S subunit (PDB entry 1S72) including the NTD of *hma*L10E was then aligned with the *eco*50S subunit with respect to the L10/L11 binding region of 23S rRNA. The NTD of *hma*L10E in this structure was subsequently used to sequentially align L10-(L12$_{NTD}$)$_4$ structures (omitting the outermost L12$_{NTD}$ dimer and its ten-residue binding segment on L10) derived from crystal structures I, II, and III of *tma*L10-(L12$_{NTD}$)$_6$ (Table S1). The fit for the helix α8-(L12$_{NTD}$)$_4$ portion was optimized by rigid-body movement relative to the L10 NTD (Figure 5 and Figure S6) around the pivot point identified in the *tma*L10-(L12$_{NTD}$)$_6$ crystal structures (Figure 2C). Similar fitting was also performed for the set of cryo-EM ribosome structures available from the EBI Database (Table S3; Figure S7).

Biochemical Procedures

Ribosomes from *E. coli* MRE 600 were prepared as described (Rodnina and Wintermeyer, 1995). Ribosomes from *T. maritima* MSB8 were prepared by the same procedure, except for opening of the cells with a French press (*T. maritima* MSB8 cells were a kind gift from K.O. Stetter, Regensburg). *eco*L12 was removed from *eco*70S ribosomes by NH$_4$Cl/ethanol treatment (Kothe et al., 2004; Mohr et al., 2002). For reconstitution, ribosome cores depleted of L12 were incubated with a 20-fold excess of purified wild-type or mutant L12 for 30 min at 37°C. AcPhe-tRNA^{Phe}, [^{14}C]Phe-tRNA^{Phe}, Phe-tRNA^{Phe}(Prf16/17), EF-Tu, and EF-G were prepared and purified as described (Kothe et al., 2004; Mohr et al., 2002).

A-site binding was studied in 50 mM Tris-HCl (pH 7.5), 70 mM NH$_4$Cl, 30 mM KCl, 10 mM MgCl$_2$, and 2 mM DTT (Kothe et al., 2004). Rapid kinetic experiments were carried out as described (Kothe et al., 2004 and Supplemental Experimental Procedures). To measure ribosome-stimulated multiple-turnover GTP hydrolysis by EF-G, ribosomes (0.05–2.0 μM) were mixed with EF-G (0.04 μM) and [γ-^{32}P]GTP (20 μM) in 50 mM Tris-HCl (pH 7.5), 70 mM NH$_4$Cl, 30 mM KCl, 7 mM MgCl$_2$, and 2 mM DTT at 37°C. Steady-state

kinetic parameters were determined under conditions of initial velocity. Exchange of L12 on the ribosomes, the copy number of L12 on *eco* and *tma* ribosomes, the ratio of ribosome bound and cytoplasmic L12, and the ratio between L12 and translation factors were determined as described in Supplemental Experimental Procedures.

Model Building

For visualization of a ribosome model (Figure 7), we used the structure of the *hma*50S subunit. Full-length *tma*L11 (PDB ID code 1MMS) was modeled by superimposing the CTDs of *tma*L11 and *hma*L11. A *tma*L10-(L12$_{NTD}$)$_4$ complex or a *tma*L10-(L12$_{NTD}$)$_6$ complex was positioned as described above for cryo-EM. We then superimposed the NMR structure of an isolated *eco*L12 dimer (PDB ID code 1RQU) on the L12$_{NTD}$ dimers of the L10-L12$_{NTD}$ complexes. Torsion angles in the unstructured hinges were adjusted to show all L12 molecules in the crown view of the 50S subunit. To indicate the location of the 30S subunit and a translation factor, we superimposed the 30S subunit from *E. coli* as seen in an *E. coli* 70S ribosome structure (PDB ID codes 1PNX and 1PNY) and EF-G according to a cryo-EM structure (PDB ID code 1JQM).

Supplemental Data

Supplemental Data include Supplemental Results and Discussion, Supplemental Experimental Procedures, Supplemental References, three tables, and seven figures and are available with this article online at http://www.cell.com/cgi/content/full/121/7/991/DC1/.

References

Agrawal, R.K., Penczek, P., Grassucci, R.A., and Frank, J. (1998). Visualization of elongation factor G on the *Escherichia coli* 70S ribosome: the mechanism of translocation. Proc. Natl. Acad. Sci. USA *95*, 6134–6138.

Agrawal, R.K., Heagle, A.B., Penczek, P., Grassucci, R.A., and Frank, J. (1999). EF-G-dependent GTP hydrolysis induces translocation accompanied by large conformational changes in the 70S ribosome. Nat. Struct. Biol. *6*, 643–647.

Agrawal, R.K., Linde, J., Sengupta, J., Nierhaus, K.H., and Frank, J. (2001). Localization of L11 protein on the ribosome and elucidation of its involvement in EF-G-dependent translocation. J. Mol. Biol. *311*, 777–787.

Ban, N., Nissen, P., Hansen, J., Moore, P.B., and Steitz, T.A. (2000). The complete atomic structure of the large ribosomal subunit at 2.4 Å resolution. Science *289*, 905–920.

Beauclerk, A.A., Cundliffe, E., and Dijk, J. (1984). The binding site for ribosomal protein complex L8 within 23S ribosomal RNA of *Escherichia coli*. J. Biol. Chem. *259*, 6559–6563.

Blanchard, S.C., Gonzalez, R.L., Kim, H.D., Chu, S., and Puglisi, J.D. (2004). tRNA selection and kinetic proofreading in translation. Nat. Struct. Mol. Biol. *11*, 1008–1014.

Bocharov, E.V., Sobol, A.G., Pavlov, K.V., Korzhnev, D.M., Jaravine, V.A., Gudkov, A.T., and Arseniev, A.S. (2004). From structure and

dynamics of protein L7/L12 to molecular switching in ribosome. J. Biol. Chem. *279*, 17697–17706.

Bourne, H.R., Sanders, D.A., and McCormick, F. (1991). The GTPase superfamily: conserved structure and molecular mechanism. Nature *349*, 117–127.

Dey, D., Bochkariov, D.E., Jokhadze, G.G., and Traut, R.R. (1998). Cross-linking of selected residues in the N- and C-terminal domains of *Escherichia coli* protein L7/L12 to other ribosomal proteins and the effect of elongation factor Tu. J. Biol. Chem. *273*, 1670–1676.

Gonzalo, P., and Reboud, J.P. (2003). The puzzling lateral flexible stalk of the ribosome. Biol. Cell. *95*, 179–193.

Harms, J., Schluenzen, F., Zarivach, R., Bashan, A., Gat, S., Agmon, I., Bartels, H., Franceschi, F., and Yonath, A. (2001). High resolution structure of the large ribosomal subunit from a mesophilic eubacterium. Cell *107*, 679–688.

Klaholz, B.P., Myasnikov, A.G., and Van Heel, M. (2004). Visualization of release factor 3 on the ribosome during termination of protein synthesis. Nature *427*, 862–865.

Kothe, U., Wieden, H.J., Mohr, D., and Rodnina, M.V. (2004). Interaction of helix D of elongation factor Tu with helices 4 and 5 of protein L7/12 on the ribosome. J. Mol. Biol. *336*, 1011–1021.

Liljas, A., and Gudkov, A.T. (1987). The structure and dynamics of ribosomal protein L12. Biochimie *69*, 1043–1047.

Mohr, D., Wintermeyer, W., and Rodnina, M.V. (2000). Arginines 29 and 59 of elongation factor G are important for GTP hydrolysis or translocation on the ribosome. EMBO J. *19*, 3458–3464.

Mohr, D., Wintermeyer, W., and Rodnina, M.V. (2002). GTPase activation of elongation factors Tu and G on the ribosome. Biochemistry *41*, 12520–12528.

Montesano-Roditis, L., Glitz, D.G., Traut, R.R., and Stewart, P.L. (2001). Cryo-electron microscopic localization of protein L7/L12 within the Escherichia coli 70 S ribosome by difference mapping and Nanogold labeling. J. Biol. Chem. *276*, 14117–14123.

Mulder, F.A.A., Bouakaz, L., Lundell, A., Venkataramana, M., Liljas, A., Akke, M., and Sanyal, S. (2004). Conformation and dynamics of ribosomal stalk protein L12 in solution and on the ribosome. Biochemistry *43*, 5930–5936.

Oleinikov, A.V., Perroud, B., Wang, B., and Traut, R.R. (1993). Structural and functional domains of Escherichia coli ribosomal protein L7/L12. The hinge region is required for activity. J. Biol. Chem. *268*, 917–922.

Pape, T., Wintermeyer, W., and Rodnina, M.V. (1998). Complete kinetic mechanism of elongation factor Tu-dependent binding of aminoacyl-tRNA to the A site of the *E. coli* ribosome. EMBO J. *17*, 7490–7497.

Rawat, U.B., Zavialov, A.V., Sengupta, J., Valle, M., Grassucci, R.A., Linde, J., Vestergaard, B., Ehrenberg, M., and Frank, J. (2003). A cryo-electron microscopic study of ribosome-bound termination factor RF2. Nature *421*, 87–90.

Rodnina, M.V., and Wintermeyer, W. (1995). GTP consumption of elongation factor Tu during translation of heteropolymeric mRNAs. Proc. Natl. Acad. Sci. USA *92*, 1945–1949.

Rodnina, M.V., Pape, T., Fricke, R., Kuhn, L., and Wintermeyer, W. (1996). Initial binding of the elongation factor Tu·GTP·aminoacyl-tRNA complex preceding codon recognition on the ribosome. J. Biol. Chem. *271*, 646–652.

Rosendahl, G., and Douthwaite, S. (1993). Ribosomal proteins L11 and L10.(L12)4 and the antibiotic thiostrepton interact with overlapping regions of the 23 S rRNA backbone in the ribosomal GTPase centre. J. Mol. Biol. *234*, 1013–1020.

Savelsbergh, A., Mohr, D., Wilden, B., Wintermeyer, W., and Rodnina, M.V. (2000). Stimulation of the GTPase activity of translation elongation factor G by ribosomal protein L7/12. J. Biol. Chem. *275*, 890–894.

Savelsbergh, A., Katunin, V.I., Mohr, D., Peske, F., Rodnina, M.V., and Wintermeyer, W. (2003). An elongation factor G-induced ribosome rearrangement precedes tRNA-mRNA translocation. Mol. Cell *11*, 1517–1523.

Stark, H., Rodnina, M.V., Wieden, H.J., van Heel, M., and Winter-meyer, W. (2000). Large-scale movement of elongation factor G and extensive conformational change of the ribosome during transloca-tion. Cell *100*, 301–309.

Stark, H., Rodnina, M.V., Wieden, H.J., Zemlin, F., Wintermeyer, W., and van Heel, M. (2002). Ribosome interactions of aminoacyl-tRNA and elongation factor Tu in the codon-recognition complex. Nat. Struct. Biol. *9*, 849–854.

Subramanian, A.R. (1975). Copies of proteins L7 and L12 and heterogeneity of the large subunit of *Escherichia coli* ribosome. J. Mol. Biol. *95*, 1–8.

Valle, M., Zavialov, A., Li, W., Stagg, S.M., Sengupta, J., Nielsen, R.C., Nissen, P., Harvey, S.C., Ehrenberg, M., and Frank, J. (2003). Incorporation of aminoacyl-tRNA into the ribosome as seen by cryo-electron microscopy. Nat. Struct. Biol. *10*, 899–906.

Vetter, I.R., and Wittinghofer, A. (1999). Nucleoside triphosphate-binding proteins: different scaffolds to achieve phosphoryl transfer. Q. Rev. Biophys. *32*, 1–56.

Vila-Sanjurjo, A., Ridgeway, W.K., Seymaner, V., Zhang, W., San-toso, S., Yu, K., and Cate, J.H. (2003). X-ray crystal structures of the WT and a hyper-accurate ribosome from Escherichia coli. Proc. Natl. Acad. Sci. USA *100*, 8682–8687.

Wahl, M.C., and Moller, W. (2002). Structure and function of the acidic ribosomal stalk proteins. Curr. Protein Pept. Sci. *3*, 93–106.

Wahl, M.C., Bourenkov, G.P., Bartunik, H.D., and Huber, R. (2000). Flexibility, conformational diversity and two dimerization modes in complexes of ribosomal protein L12. EMBO J. *19*, 174–186.

Wieden, H.-J., Wintermeyer, W., and Rodnina, M.V. (2001). A com-mon structural motif in elongation factor Ts and ribosomal protein L7/12 may be involved in the interaction with elongation factor Tu. J. Mol. Evol. *52*, 129–136.

Wimberly, B.T., Guymon, R., McCutcheon, J.P., White, S.W., and Ramakrishnan, V. (1999). A detailed view of a ribosomal active site: The structure of the L11-RNA complex. Cell *97*, 491–502.

Yusupov, M.M., Yusupova, G.Z., Baucom, A., Lieberman, K., Ear-nest, T.N., Cate, J.H.D., and Noller, H.F. (2001). Crystal structure of the ribosome at 5.5 angstrom resolution. Science *292*, 883–896.

Accession Numbers